Second International Symposium on Marine Propulsors
smp'11, Hamburg, Germany, June 2011

Numerical and Experimental Characterization of a CP Propeller Unsteady Cavitation at Different Pitch Settings

Daniele Bertetta[1], Stefano Brizzolara[3], Stefano Gaggero[3], Luca Savio[2], Michele Viviani[1]

[1]Department of Naval Architecture, Marine and Electrical Engineering (DINAEL), Genoa University, Genoa, Italy
[2] Rolls-Royce University Technology Center 'Performance in a Seaway' Department of Marine Technology, Norwegian University of Science and Technology, formerly DINAEL
[3]Marine CFD Group, Department of Naval Architecture, Marine and Electrical Engineering, Genoa University, Genoa, Italy

ABSTRACT

This paper presents results obtained in a study dedicated to the experimental and numerical investigation of the steady and unsteady hydrodynamic characteristics of a modern CP propeller including off-design operating conditions, i.e., with the blade oriented at a pitch rather far from the design value. The extensive experimental campaign has offered the opportunity to validate the accuracy of two different CFD methods: a first order unsteady panel method with some non linearities (in the Kutta condition and flow adapted wake); and a state of the art RANSE solver, Also, the unsteady conditions of the CP propeller are investigated at two very different pitch settings. The comparison of numerical predictions with experimental results shows a very good agreement of both the numerical methods with the experiments at design pitch, and also with regards to cavitation predictions. On the contrary, results at highly reduced pitch show the limits of the conventional panel method, based on potential flow solution, for which the usual viscous corrections are not any more sufficient to cope with separated viscous flow of some blade sections, which are satisfactorily modeled by the RANSE solver instead. From a careful comparison of the flow characteristics predicted by the two different numerical methods, some hypotheses for future enhancement of the panel method are formulated in the conclusions.

Keywords

CP propellers, panel methods, CFD, cavitation tunnel

1 INTRODUCTION

Propeller design has evolved significantly in last decades with the introduction of numerical methods that are able to provide a very reliable assessment of propeller characteristics. Numerical methods capability has reached very high standards, and thus, the correct prediction of unsteady cavitating conditions may be considered as a current expected requirement of modern numerical tools. Several validation studies, as for instance in Gaggero et al (2009), have demonstrated that accurate numerical predictions of steady propeller hydrodynamic characteristics can be obtained, both with a panel methods and a state-of-the-art finite volume RANSE solver over a wide range of advance coefficients on different kind of fixed pitch propellers. Nevertheless, in case of CP propellers, some additional open points still exist if "very off-design conditions" are considered; as, for example, the hydrodynamic characteristics at reduced pitches. In these conditions, the correct prediction of the flow field and pressure distribution can prove to be a significant challenge for potential flow based methods (such as panel methods) and may require the use of more sophisticated tools, like RANSE codes. Operation at a reduced pitch condition, despite being obviously less frequent and relevant for a propeller design than main operating point, may become important in particular cases, e.g., in the case of ships operated at constant RPM, thus requiring very low pitch setting when for instance approaching the harbor, and in general, also to other ships (navy ships included) when advancing at slow speed and having a requirement to keep the engine speed of revolution much higher than the idle speed. In correspondence to such cases, traditional design and analysis approaches may fail in providing sufficiently reliable predictions of propeller thrust and torque, thus representing a challenge for the designer.

In order to analyze this problem and test the limits of applicability of boundary element methods, the present paper presents the numerical and experimental characterization of a CPP at two very different settings (usual design pitch and a much reduced one). Propeller geometry and operating conditions are presented in Section 2.

CP propeller has been tested at CEHIPAR towing tank (open water tests) and at Genoa University Cavitation

Tunnel (in non-stationary functioning), as presented in Section 3. In parallel to the experimental campaign, numerical predictions of propeller characteristics have been carried out; in particular, a panel method developed at Genoa University by the Marine CFD Group (Gaggero & Brizzolara 2009) has been used, together with a commercial RANSE code already validated in different occasions (Gaggero et al 2010). The comparison of experimental measurements and numerical results is presented in Section 4, allowing us to underline the merits and the shortcomings of the two methods adopted.

2 PROPELLER CHARACTERISTICS

As anticipated, the propeller utilised for present study is a conventional CPP for a twin screw ship, which is operated at constant RPM in correspondence to very different ship speeds by means of blade pitch angle variation. The present design was derived from the existing propeller, and the main characteristics are reported in Table 1, where $P_{0.7}$ is propeller pitch at radial position r =0.7R, D and R are propeller diameter and radius, A_E is propeller expanded area, A_O is propeller disc area, and Z is blade number. The two functioning points considered in this study (in terms of ship speed V and propeller turning rate RPM) are also reported.

Table 1: Propeller main characteristics.

	Reference	Reduced
D [m]	4.6	
$P_{0.7}/D$	1.106	0.469
A_E/A_O	0.663	
Z	4	
V [kn]	abt. 24	abt. 11
RPM	abt. 180	

Complete design charts for the propeller are reported in Appendix 1.

Figure 1: Propeller model.

In order to carry out the experimental campaign, a 250 mm diameter model (Figure 1) was manufactured.

3 EXPERIMENTAL CAMPAIGN

In the present section, the experimental campaign carried out on the propeller model is summarized. The purpose of the tests was to evaluate usual propeller mechanical characteristics (thrust and torque) and cavitating behaviour (inception and extent of various phenomena).

Open water tests (Par.3.1) and cavitation tests (Par.3.3) were carried out at CEHIPAR towing tank and at DINAEL Cavitation Tunnel (Appendix 3), respectively.

In particular, at Cavitation Tunnel, the propeller has been tested simulating real functioning conditions, as follows. K&R H39 dynamometer has been used, with propeller in downstream position and longitudinal shaft inclination of about 9°. Moreover, stock shaft brackets were also included in order to simulate wake at propeller. Final test setup is reported in Figure 2.

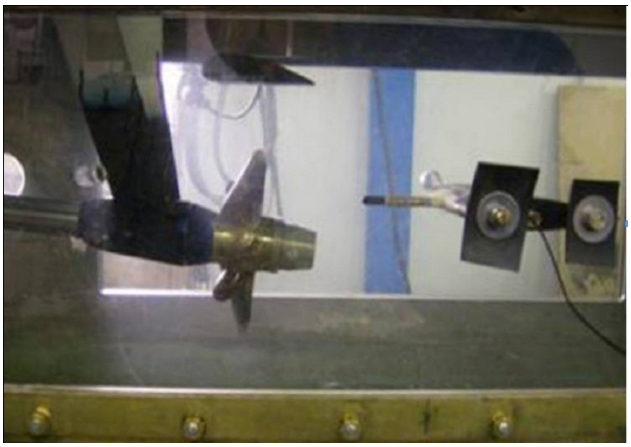

Figure 2: Test setup at cavitation tunnel.

3.1 Open Water Tests

In the following Figures 3 and 4, the results of open water tests carried out at CEHIPAR towing tank are reported, where K_T, K_Q and η_O are thrust coefficient, torque coefficient and open water efficiency, respectively.

$$K_T = {}^{T}/_{\rho N^2 D^4}$$
$$K_Q = {}^{Q}/_{\rho N^2 D^5}$$
$$\eta_o = \frac{J}{2\pi}\frac{K_T}{K_Q} \qquad (1)$$
$$J = {}^{V_A}/_{ND}$$

being T and Q propeller thrust and torque, N propeller turning rate, ρ water density, J advance coefficient and V_A advance speed at propeller. Both tests were carried out at constant RPM.

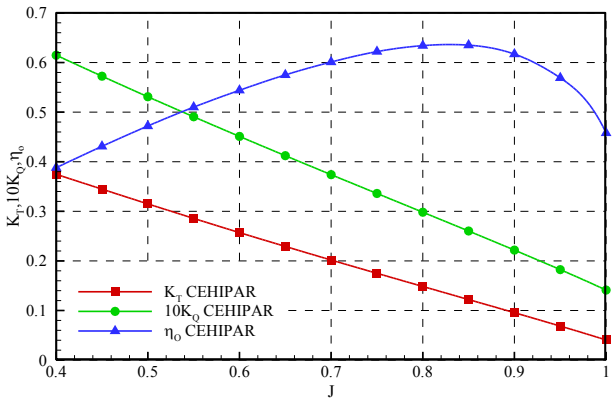

Figure 3: Open water test results, P/D = 1.106.

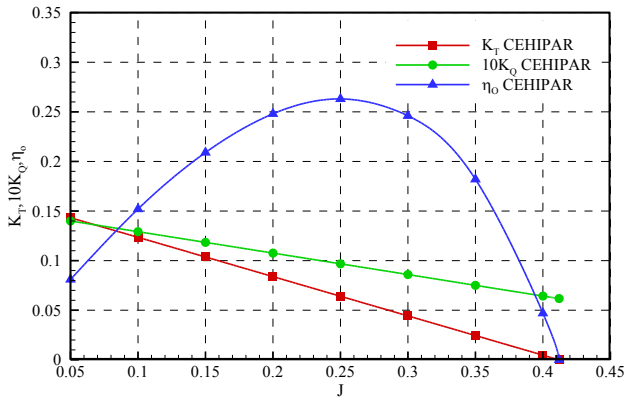

Figure 4: Open water test results, P/D = 0.469.

3.2 Wake Measurement

In order to be able to perform numerical calculations correctly reproducing experimental setup, wake measurements have been carried out by means of LDV. Wake results are reported in Figure 5; complete numerical data can be found in Appendix 2.

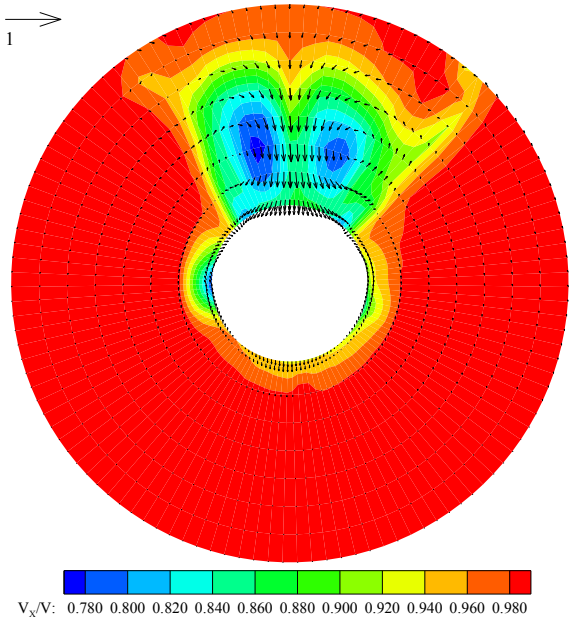

Figure 5: Non-dimensional measured wake for cavitation tests.

In Figure 5, shaft brackets wake is clearly visible, together with the more pronounced effect of inclined shaft, with two marked areas of reduced axial speed.

3.3 Cavitation Observation

For both pitches analysed, propeller cavitation bucket has been obtained at Cavitation Tunnel, with various phenomena inceptions in correspondence to different K_T values. In Figures 6 and 7, the results are summarized, where σ_N is cavitation number, defined as $(p_0 - p_{vap})/(0.5\rho N^2 D^2)$, where p_0 is pressure at propeller shaft $(p_{atm} + \rho g h)$, p_{atm} is atmospheric pressure, g is gravity acceleration, h is propeller shaft draft and p_{vap} is vapour pressure.

In both figures, the two operating conditions considered for propeller design corresponding to those indicated in Table 1, are marked with a black dot.

As expected, propeller cavitation behaviour is considerably different at the two pitches; in particular, in correspondence to reference pitch, phenomena encountered in correspondence to operating condition (K_T = 0.178, σ_N = 1.35) are tip vortex, back sheet cavitation and back bubbles at root. Bubble cavitation at tip is present only when reducing further cavitation number. Moving towards more loaded conditions, phenomena are anticipated and hub vortex is also present; while in correspondence to less loaded conditions, phenomena are delayed and face sheet cavitation is encountered. Considering reduced pitch setting, "face-related" phenomena are present, namely, vortex from sheet face and face vortex (separated from previous one); moreover, back bubbles at propeller tip and root are present in correspondence to low cavitation number. In correspondence to the operating condition analysed (K_T = 0.03, σ_N = 1.35), vortex from sheet face only is present.

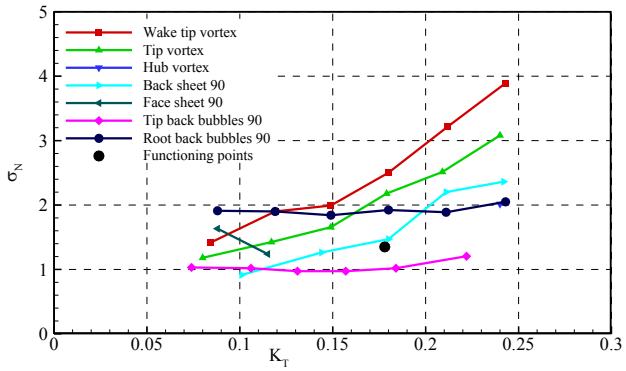

Figure 6: Cavitation phenomena inception – reference pitch.

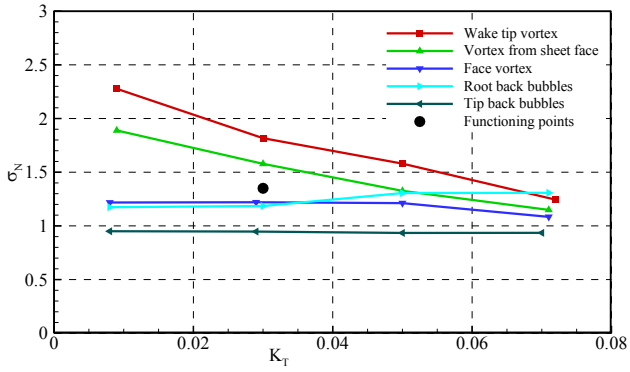

Figure 7: Cavitation phenomena inception – reduced pitch.

In parallel to cavitation inception evaluation, extension of various phenomena in correspondence to different functioning points has been visualised by means of the two cameras present during tests.

Figures related to cavitation observations in correspondence to the two functioning points indicated in the figures are directly reported together with numerical calculation results in the following section, for the sake of brevity.

4 NUMERICAL CALCULATIONS

The large amount of experimental measures in the towing tank and in the cavitation tunnel makes the tested CPP propeller an ideal candidate for the validation of the numerical codes available at the cavitation tunnel of the University of Genova. In particular, an in-house developed panel method and a commercial RANS solver (StarCCM+) have been considered. Both the solvers have been applied for the analysis of the open water non cavitating case, while only the panel method has been applied for the prediction of the cavity extension. The computational resources required to model, within the RANS approach, the whole domain that generates the inflow wake and the fully unsteady phenomena related to the cavitating flow are extremely high; thus, only the simplified potential solver has been employed to address this problem. The reference pitch condition and the reduced one have been considered in order to highlight the application limits of the two methodologies.

4.1 Panel Method

Panel/boundary elements methods model the flowfield around a solid body by means of a scalar function, the perturbation potential $\phi(x,t)$, whose spatial derivatives represent the component of the perturbation velocity vector. Irrotationality, incompressibility and absence of viscosity are the hypotheses needed in order to write the more general continuity and momentum equations as a Laplace equation for the perturbation potential itself:

$$\nabla^2\phi(\boldsymbol{x},t) = 0 \tag{2}$$

Green's third identity allows to solve the three dimensional differential problem as a simpler integral problem written for the surfaces that bound the domain. The solution is found as the intensity of a series of mathematical singularities (sources and dipoles) whose superposition models the inviscid cavitating flow on and around the body. Assuming that the cavity bubble thickness is small with respect to the profile chord, singularities that model cavity bubble can be placed on the blade surface instead than on the real cavity surface, leading to an integral equation in which the subscript q corresponds to the variable point in the integration, $\boldsymbol{n}$ is the unit normal to the boundary surfaces, and $\boldsymbol{r_{pq}}$ is the distance between points p and q. S_B is the fully wetted surface, S_W is the wake surface, and S_{CB} is the projected cavitating surface on the solid boundaries:

$$\begin{aligned} 2\pi\phi(\boldsymbol{x_p},t) &= \int_{S_B+S_{CB}} \phi(\boldsymbol{x_q},t)\frac{\partial}{\partial \boldsymbol{n}_q}\frac{1}{\boldsymbol{r}_{pq}}dS \\ &- \int_{S_B+S_{CB}} \frac{\partial\phi(\boldsymbol{x_q},t)}{\partial \boldsymbol{n}_q}\frac{1}{\boldsymbol{r}_{pq}}dS \\ &+ \int_{S_W} \Delta\phi(\boldsymbol{x_q},t)\frac{\partial}{\partial \boldsymbol{n}_q}\frac{1}{\boldsymbol{r}_{pq}}dS \end{aligned} \tag{3}$$

The set of required boundary condition is:

- Kinematic boundary condition on the wetted solid boundaries:

$$\frac{\partial\phi(\boldsymbol{x_p},t)}{\partial \boldsymbol{n}_p} = -\boldsymbol{V_{inflow}}(\boldsymbol{x_p},t)\cdot\boldsymbol{n}_p \tag{4}$$

- Kutta condition at blade trailing edge:

$$\Delta\phi_{TE}(\boldsymbol{x_p},t) = \phi^U_{TE}(\boldsymbol{x_p},t) - \phi^L_{TE}(\boldsymbol{x_p},t) \tag{5}$$

- Kelvin's theorem to drive the unsteadiness of the problem:

$$\frac{\mathcal{D}}{\mathcal{D}t}\left(\Delta\phi^w(\boldsymbol{x},t)\right) = 0 \tag{6}$$

- Dynamic boundary condition on the cavitating surfaces:

$$p = p_{vap}\ on\ S_{CB} \tag{7}$$

- Kinematic boundary condition on the cavitating surfaces (where $\boldsymbol{n}$ is the normal vector and *th* is the local cavity bubble thickness):

$$\boldsymbol{n}(\boldsymbol{x}) - th(\boldsymbol{x},t) = 0 \tag{8}$$

- Cavity closure condition at cavity bubble trailing edge.

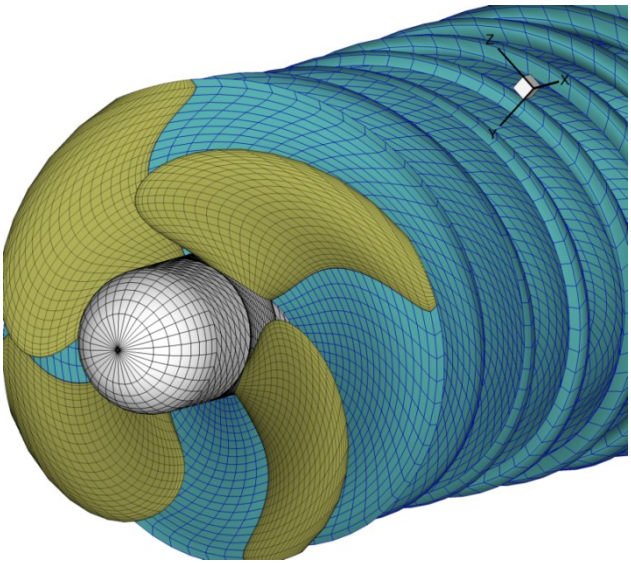

Figure 8: Panel representation of the propeller and of its trailing flow adapted wake, J = 0.8.

The numerical solution consists in an inner iterative scheme, delegated to solve the nonlinearities connected with the Kutta, the dynamic, and the kinematic boundary conditions on the unknown cavity surfaces and an outer iterative cycle stepping the time. A further force free condition for the trailing vertical wake can be employed, at least for the steady computations, requiring that each points move, from a Lagrange point of view, following:

$$\boldsymbol{x}(t) = \boldsymbol{x}(t-1) + \left(\boldsymbol{V}_{inflow} + \nabla\phi\right)\cdot\Delta t \tag{9}$$

The discretized surface mesh consists of 1500 hyperboloidal panels for each blade. The trailing vortical wake extends for six complete revolutions (needed, for the unsteady case, to reach a periodic solution) and it is

discretized with a time equivalent angular step of 6°, as in Figure 8.

4.2 RANS Solver

An analysis of open water propeller characteristics has been carried out through StarCCM+, a commercial finite volume RANS solver. Continuity and momentum equation, for an incompressible flow, are expressed by:

$$\begin{cases} \nabla \cdot \boldsymbol{U} = 0 \\ \rho \dot{\boldsymbol{U}} = -\nabla p + \mu \nabla^2 \boldsymbol{U} + \nabla \cdot \boldsymbol{T}_{Re} + \boldsymbol{S}_M \end{cases} \quad (10)$$

in which $\boldsymbol{U}$ is the averaged velocity vector, p is the averaged pressure field, μ is the dynamic viscosity, $\boldsymbol{S_M}$ is the momentum sources vector and $\boldsymbol{T_{Re}}$ is the tensor of Reynold stresses, computed in agreement with the $k-\varepsilon$ turbolence model. The computational domain, by means of the symmetries, is represented by an angular sector of amplitude $2\pi/Z$ around a single blade, discretized with an unstructured mesh of 1M polyhedral cells, as in Figure 9.

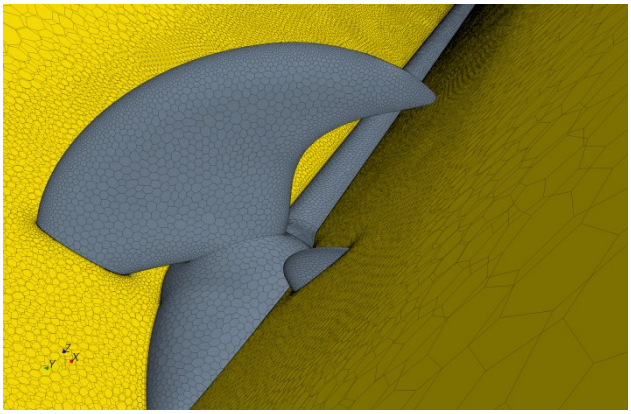

Figure 9: RANS polyhedral mesh of the propeller. 1M cells for each blade sector.

4.3 Results

Experimental campaign has been numerically reproduced, addressing both pitches. In Paragraph 4.3.1, open water tests in stationary flow are considered; while in Paragraph 4.3.2, cavitating behavior in non-uniform wake is assessed, considering, in particular, cavitation extension.

4.3.1 Open water tests

Figures 10 and 11 show the comparison between towing tank measures and numerical computations for the open water test case for both the selected pitches. At the reference pitch, the overall agreement between measures and the numerical codes is satisfactory. For what regards the thrust coefficient, both the panel method and the RANS solver accurately predict measured values: RANS computations, in particular, are very close to the towing tank measures (error lower than 3%); while potential theory presents a slightly higher discrepancy (about 5%), especially at higher values of advance coefficient. For what regards torque, numerical computations are close each other but a bit overestimated with respect to experiments; nevertheless, curve slope is correctly captured. For lower values of advance coefficient panel method torque curve has a change in slope that is related to the leading edge separation forces, whose influence for higher values of angle of attack is not negligible; potential approach is not able to compute this except through empirical corrections.

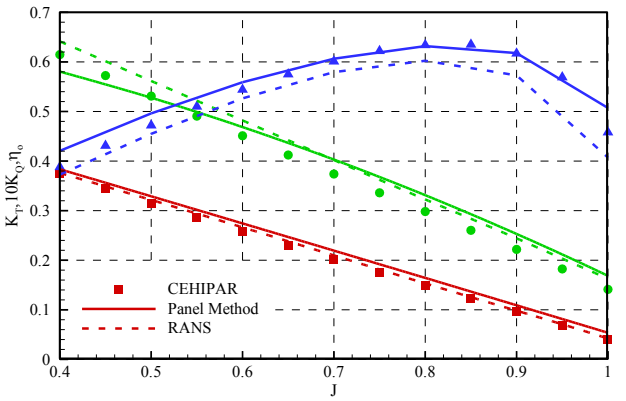

Figure 10: Comparison between experiments, panel method and RANS numerical results, reference pitch.

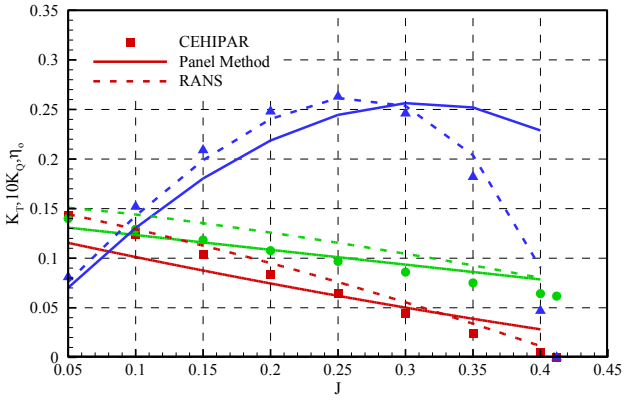

Figure 11: Comparison between experiments, panel method and RANS numerical results, reduced pitch.

At the reduced pitch, differences are higher, especially for what regards potential computations. Thrust and torque curves computed with the potential theory have different slopes with respect to the measured ones: although at the working point (between J = 0.3 and J = 0.35), in correspondence of which cavitating computations and observations have been carried out, differences are not so high, for lower values of advance coefficient panel method underpredicts both thrust and torque, while for higher values of J it overestimates them, with a zero thrust point well higher than the measured one. The application of the force free condition on the vortical trailing wake, which was the key point at the reference pitch to obtain accurate predictions of the propeller characteristics, does not reasonably improve the computations.

On the other hand, RANS computed thrust and torque curves, although a bit overpredicted, have the right slope, with almost the same zero thrust point. As for the reference pitch condition, torque prediction is the critical aspect of the numerical approach. The RANS analysis of the flowfield can suggest reasons for these differences. In Figures 12 and 13, for instance, regions with low values of Wall Shear Stress are highlighted, together with on-

body streamlines computed via RANS and Panel Method. Even if wall shear stress is always greater than zero near the hub, at the blade trailing edge it reaches values very close to the separation limit, suggesting that separation could occur. Both the reference and the reduced pitch configurations, however, are subjected to this phenomenon, with comparable magnitude and extension. Its effect on thrust and torque, even if limited, is naturally more relevant at the reduced pitch condition: the potential approximation, not able to capture separation, results in a small error at reference pitch; this error becomes non negligible with respect to the lower values of thrust and torque delivered at the reduced pitch. RANS streamlines analysis, moreover, identifies this recirculation region, completely ignored by the panel method, and which contributes to increase the cross flow on the blade. In fact, as from Figure 13, RANSE all streamlines from blade root until about 0.7 r/R show curved paths that converge toward the blade tip, while potential flow ones are significantly less affected by this outward cross flow. From the hydrodynamic point of view, the effect of the cross flow in this region changes the effective hydrodynamic chord, pitch and camber distribution along the blade, from those geometrically defined for sections at constant radius to the "effective" (hydrodynamic) ones obtained from that real flow on the blade. In particular, in the case of Figure 13, in the region of 0.4R-0.7R the chord, pitch and camber of effective RANSE blade profiles are increased with respect to that of the potential flow solution, thus justifying the difference obtained on torque and thrust predictions.

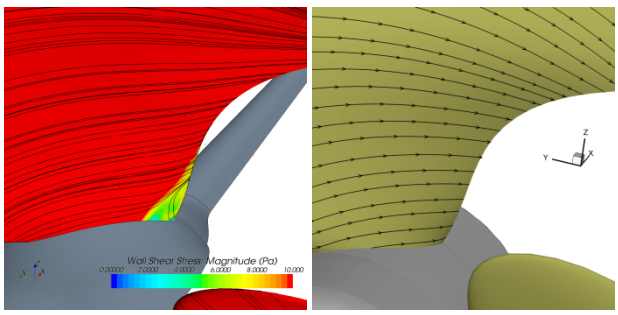

Figure 12: Wall shear stress and streamlines for the reference pitch. RANS vs. Panel Method at J = 0.8.

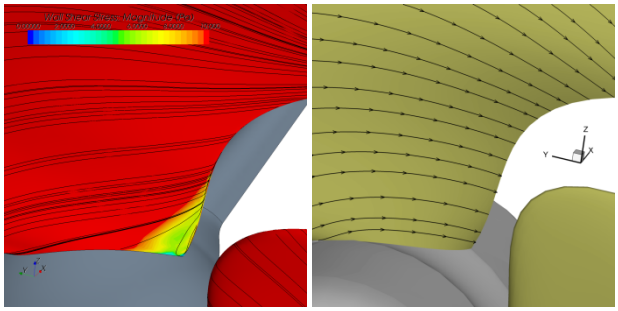

Figure 13: Wall shear stress and streamlines for the reduced pitch. RANS vs. Panel Method at J = 0.1.

4.3.2 Cavitation Extension

In Figures 15 and 16, comparison of numerical and experimental results for cavitation extension at

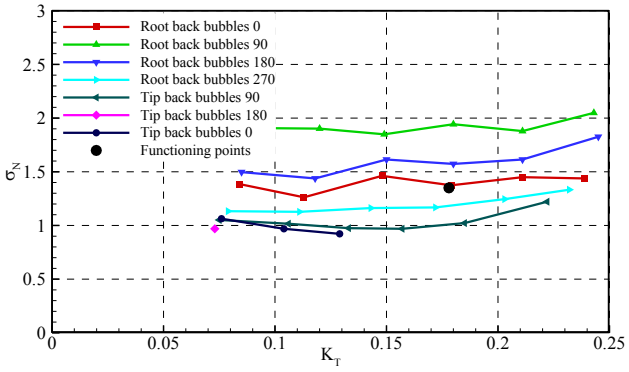

Figure 14: Bubble phenomena inception at different angular position.

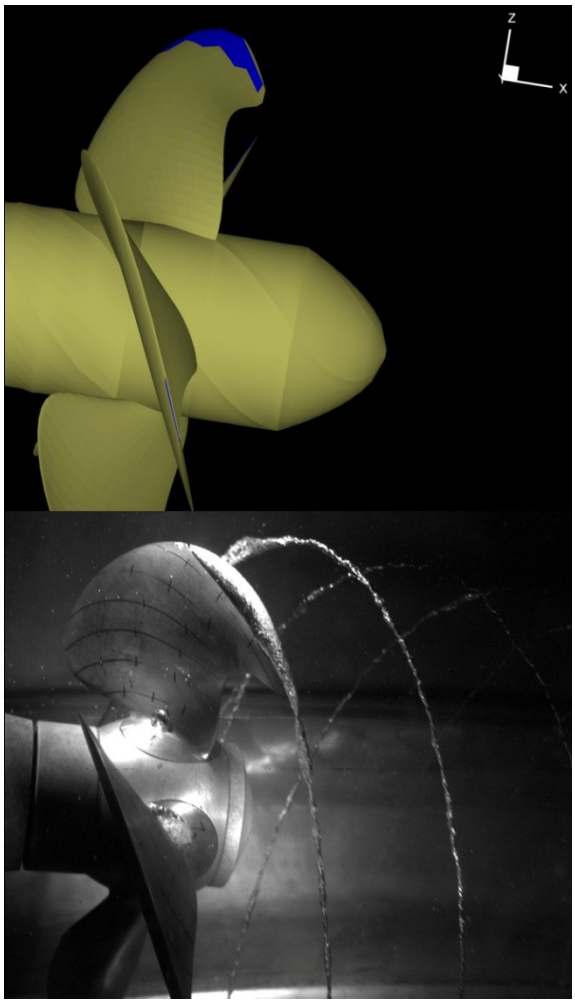

Figure 15: Cavitation extension for the reference pitch, 0° angular position.

reference pitch in correspondence to 0° and 90° angular positions respectively are reported.

As it can be seen, back sheet cavitation extension is reproduced correctly for both angular positions; moreover, at 90° position root back bubbles are also

evidenced (even if not clearly visible in the figure from experiments). This is consistent with cavitation bucket when different inception values are considered at different angular positions (see Figure 14); as it can be seen, at

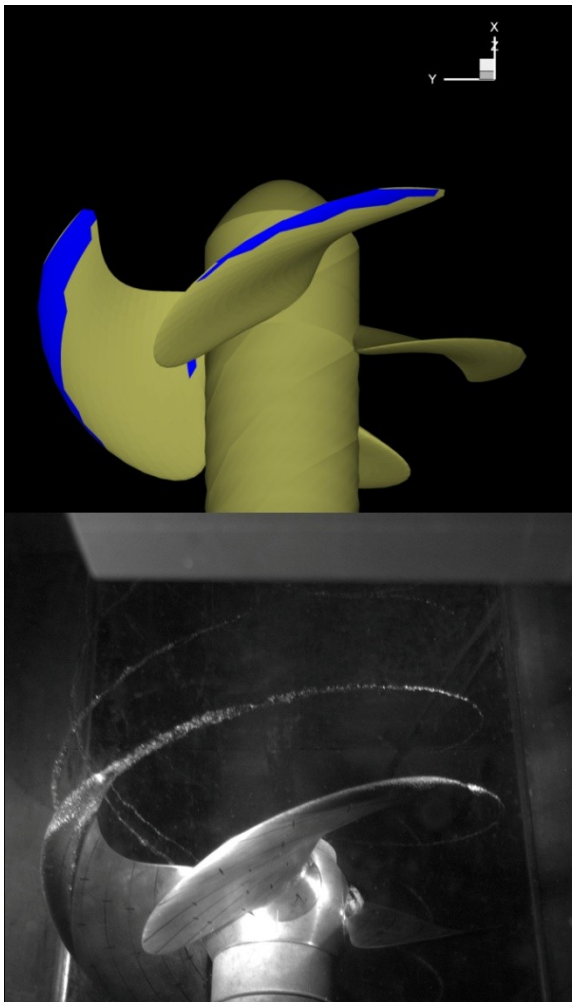

Figure 16: Cavitation extension for the reference pitch, 90° angular position.

considered functioning point root bubbles are present in correspondence to 90° and 180° angular position.

In Figure 17, comparison of cavitation extension in correspondence to reduced pitch condition is reported. In this case, a very limited cavitation is evidenced in the numerical calculations; this corresponds to the vortex from sheet face phenomenon, even if extension is, in this case, slightly overestimated. Taking into account the very off design nature of this condition, however, results are considered satisfactory.

5 CONCLUSIONS

A complete experimental and numerical analysis of a CPP propeller has been carried out. Open water and cavitation measurements have been performed and two numerical solvers have been validated in steady non cavitating and unsteady cavitating conditions. Results show very low errors at reference pitch, while at reduced pitch, as expected, limits of the panel method in such extreme conditions are highlighted. In particular, different curve slopes are predicted, and a general underestimation of thrust and overestimation of torque appears.

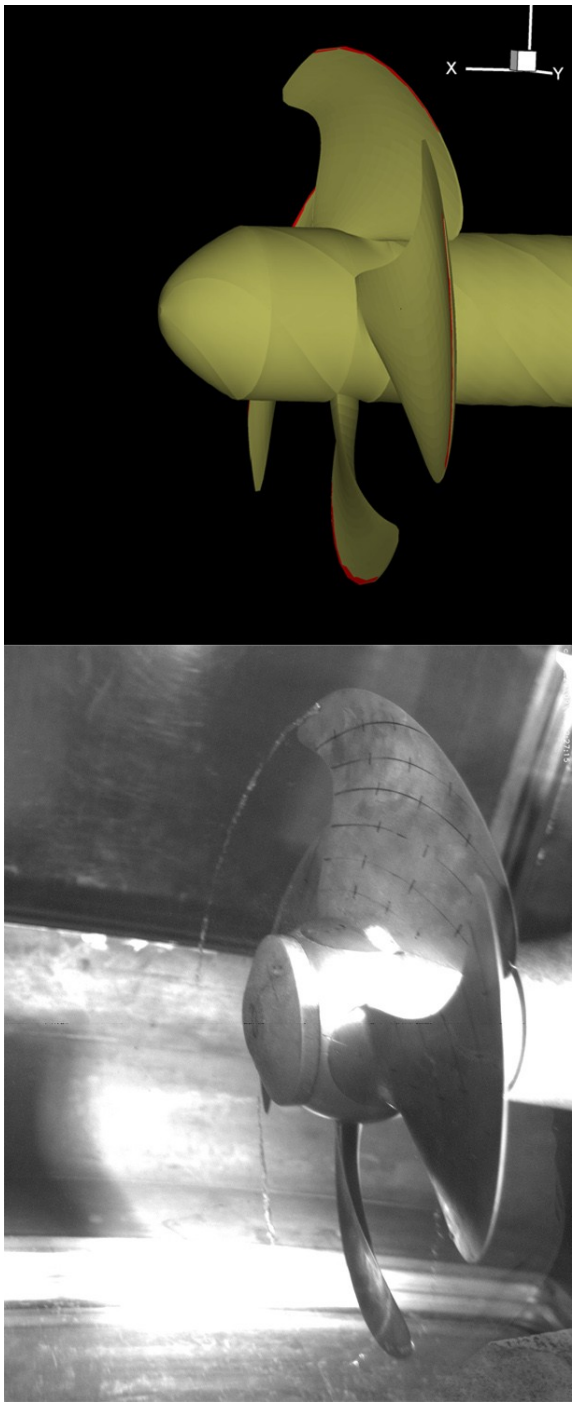

Figure 17: Cavitation extension for the reduced pitch, 0° angular position.

On the contrary, RANS is capable of evaluating thrust and torque curves slope correctly, with minor differences for the thrust and slightly overestimated values for the torque.

In order to reduce discrepancy found for potential code, a simple thin boundary layer solver, able to approximate separated regions, iteratively coupled with the inviscid solution, could be useful. Regarding the RANS solver, the application of more accurate turbulent models ($k-\omega$ or RST) could reduce differences with measured values and improve torque prediction.

It is believed that both solvers can be considered a good starting point for the numerical analysis of CPP propellers, also at extremely low values of pitch: the computational efficiency of the panel method, together with its sufficient accuracy (at least in comparative terms), allows its application as a design tool in large optimization procedures where computational time has to be limited; on the contrary, the superior accuracy of RANS solver made this approach suitable for a final and more precise analysis, and verification of panel code results.

Unsteady cavitating phenomena, observed at the cavitation tunnel of the University of Genova, are also captured by the potential solver with sufficient accuracy, both at reference pitch, with back sheet and bubble cavitation extension at different angular positions well captured, and at reduced pitch, with a thin face leading edge cavity in place of the vortex from face cavitation. Considering the inability of the developed panel method to compute vortex cavitation, the results are satisfactory and demonstrate that a computationally efficient approach like potential theory can also be employed for the analysis of unsteady cavitating flows.

ACKNOWLEDGEMENT

The present work has been carried out in the framework of Project "Ships oriented Innovative soLutions to rEduce Noise & Vibrations" (SILENV), financed by EU in the FP7-TRANSPORT.

REFERENCES

Gaggero, S. & Brizzolara, S. (2009). 'A Panel Method for Trans-Cavitating Marine Propellers'. Proceedings of the 7th International Symposium on Cavitation, Ann Arbor, Michigan, United States.

Gaggero, S., Villa, D. & Brizzolara, S. (2010). 'RANS and Panel Method for Unsteady Flow Propeller Analysis'. Proceedings of the 9th International Conference on Hydrodynamics, Shanghai, China.

Gaggero, S., Savio, L., Brizzolara, S., Viviani, M., Ferrando, M. & Conti, F. (2009). 'Comparison of experimental measurements and numerical calculations for a propeller in axial cylinder'. First International Symposium on Marine Propulsion, Trondheim, Norway.

Grassi, D., Brizzolara, S., Viviani, M., Savio, L. & Caviglia, S. (2010). 'Design and Analysis of Counter-Rotating Propellers – Comparison of Numerical and Experimental Results'. 9th International Conference on Hydrodynamics, Shanghai, China.

Savio, L., Viviani, M., Conti, F. & Ferrando, M. (2009). 'Application of computer vision techniques to measure cavitation bubble volume and cavitating tip vortex diameter'. Proceedings of the 7th International Symposium on Cavitation, Ann Arbor, Michigan, USA.

Savio, L., Viviani & Ferrando, M. (2009). 'Propeller Cavitation 3d Reconstruction through Stereo-Vision Algorithms'. Proceedings of the 1st International Conference on Advanced Model Measurement Technology for the EU Maritime Industry, Nantes, France.

Savio, L., Pittaluga, C., Viviani, M., Ferrando, M. & Conti, F. (2008). 'An Experimental and Numerical Study on Cavitation of Hull Appendages'. 6th International Conference On High-Performance Marine Vehicles, Naples, Italy.

APPENDIX 1 PROPELLER DESIGN CHART

Propeller design chart is reported in Table A-1, where c is propeller chord, t_{max} is maximum sectional thickness and f_{max} is maximum camber.

Table A-1: Propeller design chart.

r/R	c/D	skew [°]	rake/D	P/D	t_{max}/c	f_{max}/c
0.30	0.166	0.000	0.000	0.852	0.301	0.011
0.35	0.236	-7.011	-0.017	0.905	0.198	0.015
0.40	0.296	-12.133	-0.031	0.952	0.142	0.018
0.50	0.388	-17.296	-0.054	1.031	0.079	0.023
0.60	0.447	-16.487	-0.065	1.083	0.047	0.026
0.70	0.471	-10.448	-0.062	1.106	0.032	0.024
0.80	0.455	0.183	-0.037	1.097	0.026	0.018
0.90	0.380	14.689	0.012	1.052	0.026	0.011
0.95	0.303	22.931	0.043	1.016	0.027	0.007
1.00	0.000	30.450	0.073	0.971	0.029	0.002

Table A-2: Propeller profile.

x/c	0	0.0039	0.0157	0.0351	0.0618	0.0955	0.1355	0.1813
$t/2t_{max}$	0	0.0566	0.1416	0.2042	0.2637	0.3182	0.3667	0.4086
f/f_{max}	0	0.0344	0.1093	0.2070	0.3177	0.4341	0.5498	0.6599

x/c	0.2871	0.3455	0.4063	0.4686	0.5314	0.5937	0.6545	0.7129
$t/2t_{max}$	0.4706	0.4893	0.4989	0.4985	0.4874	0.4654	0.4337	0.3936
f/f_{max}	0.8463	0.9157	0.9657	0.9942	1.0000	0.9819	0.9387	0.8724

x/c	0.8187	0.8645	0.9045	0.9382	0.9649	0.9843	0.9961	1
$t/2t_{max}$	0.2948	0.2402	0.1848	0.1311	0.0817	0.0400	0.0108	0
f/f_{max}	0.6483	0.4920	0.3415	0.2149	0.1177	0.0508	0.0124	0

APPENDIX 2 WAKE MEASUREMENTS

In Table A-2, wake measurements are reported. In particular, non-dimensional values of the three velocity components $(1-w)_{\frac{r}{R},\theta}$ are given in correspondence to different radial and angular positions, where:

$$(1-w)_{\frac{r}{R},\theta} = \frac{V\left(\frac{r}{R},\theta\right)}{V} \qquad \text{(A-1)}$$

Table A-3: Wake measurements – x velocity component.

θ	r/R				
	0.3	0.5	0.7	0.9	1.1
0	0.8596	0.8563	0.9385	0.9698	0.9727
10	0.8639	0.8194	0.8664	0.9687	0.9830
20	0.8601	0.7789	0.8833	0.9783	0.9832

30	0.8575	0.8341	0.9196	0.9823	0.9843
40	0.8189	0.8876	0.9381	0.9813	0.9510
50	0.8987	0.9502	0.9677	0.9835	0.9838
60	0.9543	0.9815	0.9861	0.9847	0.9837
70	0.9408	0.9837	0.9865	0.9841	0.9859
80	0.9349	0.9855	0.9884	0.9888	0.9882
90	0.9342	0.9861	0.9899	0.9901	0.9897
100	0.9135	0.9895	0.9915	0.9928	0.9912
110	0.9052	0.9912	0.9949	0.9895	0.9907
120	0.9315	0.9915	0.9917	1.0001	1.0001
130	0.9404	0.9904	1.0000	1.0001	1.0001
140	0.9441	0.9992	1.0001	1.0001	1.0001
150	0.9464	0.9992	1.0001	1.0001	1.0001
160	0.9493	0.9991	1.0001	1.0001	1.0001
170	0.9467	1.0001	1.0001	1.0001	1.0001
180	0.9438	0.9993	1.0000	1.0000	1.0000
190	0.9480	0.9994	1.0000	1.0000	1.0000
200	0.9513	0.9995	1.0000	1.0000	1.0000
210	0.9599	0.9997	1.0000	1.0000	1.0000
220	0.9640	0.9997	1.0000	1.0000	1.0000
230	0.9647	0.9999	1.0000	1.0000	1.0000
240	0.9556	1.0015	1.0001	1.0000	1.0000
250	0.9107	1.0000	0.9995	0.9966	0.9938
260	0.8443	0.9965	0.9985	0.9967	0.9952
270	0.8136	0.9951	0.9970	0.9953	0.9938
280	0.8395	0.9937	0.9930	0.9923	0.9922
290	0.8891	0.9920	0.9914	0.9905	0.9920
300	0.9231	0.9886	0.9906	0.9889	0.9889
310	0.9541	0.9854	0.9874	0.9873	0.9873
320	0.8577	0.9650	0.9853	0.9739	0.9873
330	0.8163	0.8538	0.9103	0.9766	0.9636
340	0.8431	0.8009	0.8452	0.9733	0.9824
350	0.8452	0.7790	0.8369	0.9673	0.9820
360	0.8596	0.8563	0.9385	0.9698	0.9727

Table A-4: Wake measurements – y velocity component.

θ	r/R				
	0.3	0.5	0.7	0.9	1.1
0	-0.0082	0.0258	0.0164	-0.0033	-0.0059
10	0.0362	0.0045	-0.0684	-0.0592	-0.0306
20	0.0694	0.0158	-0.1026	-0.0747	-0.0446
30	0.0854	0.0601	-0.0663	-0.0667	-0.0470
40	0.0532	0.0718	-0.0207	-0.0582	-0.0454
50	-0.0502	0.0130	0.0077	-0.0138	-0.0407
60	-0.0556	-0.0125	-0.0048	-0.0101	-0.0231
70	-0.0474	-0.0167	-0.0124	-0.0149	-0.0230
80	-0.0099	-0.0144	-0.0143	-0.0169	-0.0229
90	0.0070	-0.0091	-0.0123	-0.0150	-0.0230
100	0.0000	0.0000	0.0000	0.0000	0.0000
110	0.0000	0.0000	0.0000	0.0000	0.0000
120	0.0000	0.0000	0.0000	0.0000	0.0000
130	0.0000	0.0000	0.0000	0.0000	0.0000
140	0.0000	0.0000	0.0000	0.0000	0.0000
150	0.0000	0.0000	0.0000	0.0000	0.0000
160	0.0000	0.0000	0.0000	0.0000	0.0000
170	0.0000	0.0000	0.0000	0.0000	0.0000
180	0.0000	0.0000	0.0000	0.0000	0.0000
190	0.0000	0.0000	0.0000	0.0000	0.0000
200	0.0000	0.0000	0.0000	0.0000	0.0000
210	0.0000	0.0000	0.0000	0.0000	0.0000
220	0.0000	0.0000	0.0000	0.0000	0.0000
230	0.0000	0.0000	0.0000	0.0000	0.0000
240	0.0000	0.0000	0.0000	0.0000	0.0000
250	0.0000	0.0000	0.0000	0.0000	0.0000
260	0.0000	0.0000	0.0000	0.0000	0.0000
270	-0.0321	0.0111	0.0189	0.0202	0.0185
280	0.0127	0.0222	0.0234	0.0222	0.0190
290	0.0614	0.0311	0.0264	0.0231	0.0192
300	0.0733	0.0347	0.0312	0.0224	0.0188
310	0.0609	0.0318	0.0381	0.0193	0.0152
320	0.0171	0.0163	0.0605	-0.0073	0.0165
330	-0.0585	-0.0082	0.0310	0.0061	0.0178
340	-0.0757	0.0142	0.0774	0.0439	0.0226
350	-0.0455	0.0395	0.0831	0.0449	0.0134
360	-0.0082	0.0258	0.0164	-0.0033	-0.0059

Table A-5: Wake measurements – z velocity component.

θ	r/R				
	0.3	0.5	0.7	0.9	1.1
0	-0.1947	-0.3205	-0.2158	-0.1007	-0.0567
10	-0.1786	-0.2702	-0.1429	-0.0605	-0.0285
20	-0.1394	-0.1359	-0.0251	-0.0146	-0.0119
30	-0.0951	0.0312	0.0624	0.0106	0.0054
40	-0.0538	0.0720	0.0685	-0.0031	0.0376
50	-0.0233	0.0384	0.0340	0.0562	0.0446
60	0.0186	0.0296	0.0318	0.0423	0.0396
70	0.0647	0.0349	0.0355	0.0375	0.0361
80	0.0779	0.0422	0.0376	0.0362	0.0339
90	0.0757	0.0449	0.0385	0.0346	0.0317
100	0.0787	0.0445	0.0384	0.0336	0.0296
110	0.0623	0.0432	0.0372	0.0323	0.0284
120	0.0481	0.0371	0.0355	0.0003	0.0003
130	0.0267	0.0315	0.0160	0.0003	0.0003
140	0.0000	0.0015	0.0003	0.0003	0.0003
150	-0.0256	0.0006	0.0003	0.0003	0.0003
160	-0.0473	0.0002	0.0003	0.0003	0.0003
170	-0.0631	0.0003	0.0003	0.0003	0.0003
180	-0.0861	-0.0015	-0.0001	-0.0001	-0.0001
190	-0.0787	-0.0013	-0.0001	-0.0001	-0.0001
200	-0.0612	-0.0008	-0.0001	-0.0001	-0.0001
210	-0.0353	-0.0003	-0.0001	-0.0001	-0.0001
220	-0.0028	0.0004	-0.0001	-0.0001	-0.0001
230	0.0355	0.0181	0.0054	-0.0001	-0.0001
240	0.0641	0.0266	0.0159	-0.0001	-0.0001
250	0.0802	0.0317	0.0196	0.0120	0.0067
260	0.0763	0.0369	0.0212	0.0119	0.0081
270	0.0744	0.0410	0.0227	0.0126	0.0085
280	0.0703	0.0378	0.0227	0.0136	0.0083
290	0.0399	0.0325	0.0206	0.0095	0.0082
300	0.0101	0.0258	0.0184	0.0063	0.0048
310	-0.0250	0.0262	0.0166	-0.0031	0.0039
320	-0.0602	0.0470	0.0177	-0.0371	-0.0008
330	-0.0791	0.0506	0.0580	-0.0103	-0.0257
340	-0.1237	-0.0493	0.0199	-0.0122	-0.0295
350	-0.1708	-0.2329	-0.1205	-0.0629	-0.0423
360	-0.1947	-0.3205	-0.2158	-0.1007	-0.0567

It has to be noted that x, y, and z components are referred to undisturbed flow direction (not to propeller reference system) being longitudinal, lateral and vertical components respectively, as schematically represented in Figure A.1.

APPENDIX 3: CAVITATION TUNNEL

The Cavitation Tunnel facility of the Department of Naval Architecture and Electrical Engineering of the University of Genoa (DINAEL) is schematically represented in Figure A.2.

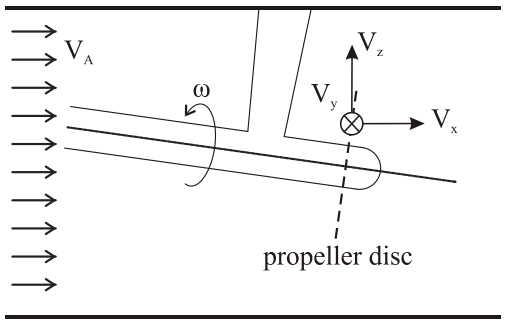

Figure A.1: Reference system for LDV measurements.

The facility is a Kempf & Remmers closed water circuit tunnel with a squared testing section of 0.57 m x 0.57 m, having a total length of 2 m. The nozzle contraction ratio is 4.6:1, and the maximum flow speed in the testing section is 8.5 m/s.

Vertical and horizontal distances between ducts are 4.54 m, and 8.15 m, respectively.

The tunnel is equipped with a Kempf & Remmers H39 dynamometer, which measures propeller thrust, torque and RPM. Flow speed in the testing section is measured by means of a differential venturi-meter with two pressure plugs immediately upstream and downstream of the converging part. A mobile stroboscopic system allows to visualise cavitation phenomena on the propeller blades. In addition to this, a certain number (usually two/three) of cameras. Allied Vision Tech Marlin F145B2 Firewire Cameras, with a resolution of 1392 x 1040 pixels and a frame rate up to 10 fps are currently adopted. Recent research activity has led to the development of a novel technique, based on computer vision, for the measurement of sheet cavitation volume and tip vortex diameter (Savio et al 2009a and 2009b). The Cavitation Tunnel is also equipped with instrumentation for non-intrusive measurement of velocity field, i.e., Laser Doppler Velocimetry (LDV). During all tests, oxygen content is constantly monitored by means of ABB dissolved oxygen sensor model 8012/170, together with analyser ABB AX400. Constant testing conditions in terms of oxygen content are utilised in order to have a fair comparison of propellers.

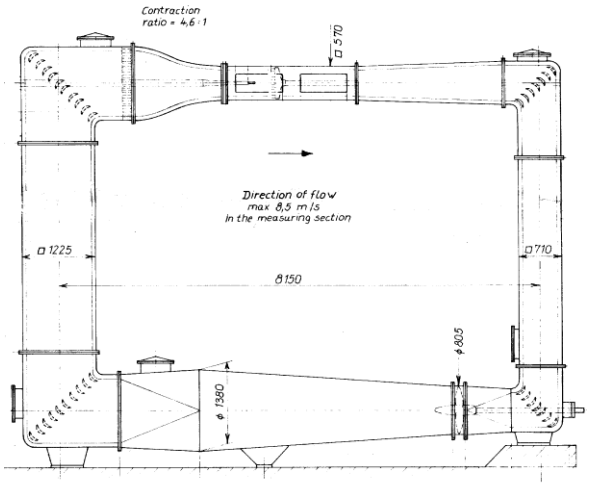

Figure A.2: DINAEL cavitation tunnel layout.

DINAEL Cavitation Tunnel is utilised for conventional industrial tests, for development of new testing techniques (like previously mentioned computer vision techniques) and for validation of numerical codes results (Savio et al 2008, Gaggero et al 2009, Grassi et al 2010).